Numerical Evaluation of Climate Scatter Performance of a Cycloidal Wave Energy Converter

Kedar C. Chitale, Casey Fagley, Ali Mohtat, Stefan G. Siegel

Abstract—**Ocean waves offer an uninterrupted, rich resource of globally available renewable energy. However, because of their high cost and low power production, commercial wave energy converters are not operational at present. In this paper, we numerically evaluated the performance of a novel feedback-controlled lift-based cycloidal wave energy converter (CycWEC) at various sea states of the Humboldt Bay wave climate. The device comprised of two hydrofoils attached eccentrically to a shaft at a radius, submerged at a distance under the ocean surface. The pitch of the blades was feedback-controlled based on estimation of the incoming wave. The simulations were performed for regular waves and irregular waves approximated with a JONSWAP spectrum. Climate data from Humboldt Bay, CA was used to estimate the yearly power generation. The results underline the importance of a well-tuned control algorithm to maximize the annual energy production. The estimated annual energy production of the CycWEC was 3000MWh from regular wave simulations and 1800MWh from irregular wave simulations, showing that it can be a commercially viable means of electricity production from ocean waves.**

Keywords—**Wave Energy Converter, Numerical Simulations, Irregular Waves, Wave Climate Scatter**

I. Introduction

The oceans cover 70% of the surface of the earth. Ocean waves are a potential uninterrupted, rich and abundant source of renewable energy that is globally available [1]. However, because of the high cost and technical challenges such as low energy production, there are currently only a handful commercially operational wave power plants. One of the grids connected wave energy converters is at Mutriku, in Spain, in operation since 2011 [2]. The research on wave energy converters has been going on for many years and a lot of designs have tried and failed at producing commercially viable wave power at scale. Comprehensive reviews of different wave energy converters (WEC) can be found in McCormick [3], Cruz [4] and Rusu [5].

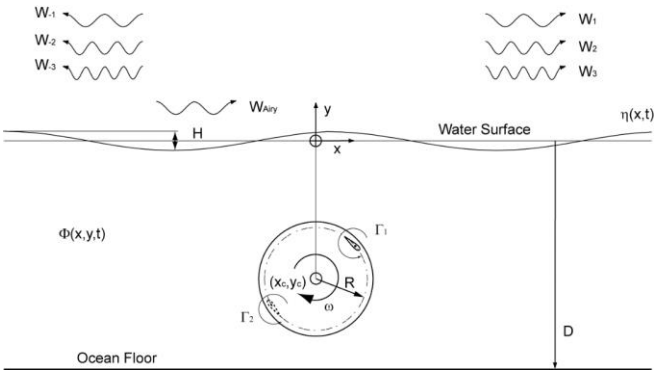

Fig. 1. Representation of the CycWEC geometry [6].

Relative to other types of WECs, lift-based wave termination devices have not been researched extensively. Wu [6] analysed the interaction of an oscillating hydrofoil with waves, concluding that a net energy gain is possible. For the application of alternative energy, initial investigations of lift-based wave energy conversion by means of a single hydrofoil were performed at TU Delft as early as the 1990s [7]. A major advantage of this approach over traditional WECs is that the wave energy can be converted directly into rotational mechanical energy, as noted by Hermans et al. [8]. This initial work showed the feasibility of a cycloidal wave energy converter to self-synchronize with the incoming wave in terms of rotational phase. However, the conversion efficiencies in the theoretical work conducted at TU Delft and the wave tunnel experiments performed at MARIN were very small, on the order of a few percent in experiments, with an estimated theoretical maximum of 15%.

Manuscript submitted 24 December, 2021; published 19 December 2022. This work was supported in part by the Department of Energy under grant EE0008626.

K. C. Chitale is a Principal CFD Engineer at Atargis Energy Corporation, 1111 Lavender Way, Pueblo CO 81001, USA (e-mail: kedar.chitale@atargis.com).

C. Fagley is the Chief Controls Engineer at Atargis Energy Corporation (email: casey.fagley@atargis.com)

A. Mohtat is a Principal Ocean Engineer at Atargis Energy Corporation (email: ali.mohtat@atargis.com)

S. G. Siegel is the Chief Technology Officer at Atargis Energy Corporation (email: stefan.siegel@atargis.com)

Digital Object Identifier: https://doi.org/10.36688/imej.5.315-326

More recently, Siegel et al. [9] showed through simulations that with improved sizing of the WEC and by using synchronization of the rotation of the foil with the incoming harmonic wave, wave termination with better than 99% inviscid efficiency was possible. Experiments at the 1:300 scale validated these findings in 2011 [10]. Later the experimental investigation advanced to a scale of 1:10 in a 3-D wave basin [11]. At this scale, electricity was successfully produced and quantitatively measured for the first time. The experiments also showed these WECs to be relatively insensitive to angular misalignment with the incoming wave crests. Jeans et al. [12] numerically evaluated performance of the CycWEC in cancelling irregular waves based on a Bretschneider spectrum consisting of 7 to 10 wave components and showed inviscid efficiencies over 80%. Siegel et al. experimentally achieved wave cancellation of irregular waves with 60-80% efficiency as measured from the wave gauges [13]. Siegel et al. [14] calculated the effect of different design parameters on overall performance of the CycWEC for the Mokapu Point wave climate.

The simulations of the CycWEC so far have mostly focused on its inviscid performance. To calculate the practical power conversion, drag losses need to be properly estimated, including parasitic and induced drag effects. The performance of the CycWEC diminishes significantly once these losses are included, compared to the inviscid results. To solve this problem, a new control strategy is needed to minimize these losses and increase power production. Also, the wave cancellation needs to be evaluated at multiple sea states to estimate the performance of the CycWEC at sea. This can be achieved by using buoy data from a certain location to calculate annual power production. In the end, the performance needs to be evaluated for irregular waves with an improved spectrum resolution compared to the earlier results.

In this paper, regular and irregular wave cancellation were simulated at multiple wave conditions with two different control strategies. The Humboldt Bay wave climate data was used to predict yearly energy generation and bulk efficiency.

II. Numerical Approach

The numerical scheme was based on a 2-dimensional potential flow approximation of the inviscid Navier-Stokes equations (Euler equations). Under these assumptions, the governing continuity equation simplified to the Laplace equation.

The numerical model predicted waves generated by the CycWEC and their interaction with an incoming wave to calculate the wave cancellation efficiency based on potential flow model. The hydrofoils were numerically represented with point vortices of strengths equal to the circulation of the hydrofoil. Viscous drag losses were estimated using externally calculated lift to drag relationship (drag polar) of the hydrofoil. The following sections outline the mathematical details of the numerical model and the CycWEC geometry.

A. CycWEC geometry

A two-dimensional sketch of a typical CycWEC as considered in this paper, is shown in Fig. 1. It features two hydrofoils attached parallel to a horizontally oriented main shaft at a radius R, rotating clockwise at an angular speed ω, and is submerged at a depth y_c, which was measured relative to a Cartesian coordinate system with y=0 being the undisturbed free surface [9]. The orientation (pitch) of each hydrofoil was adjusted to produce the desired level of circulation Γ. At any point on the free surface the vertical elevation was η and peak-to-trough amplitude of the resulting wave field was H. The incoming ocean waves were assumed to travel in the positive X direction as shown in Fig. 1. The water depth D was assumed infinite, i.e., deep water waves were investigated.

The geometry parameters of the CycWEC at ocean scale used in this analysis are given in Table 1. A detailed study on optimization of the WEC geometry parameters can be found in [14].

TABLE 1
GEOMETRY PARAMETERS OF THE CYCWEC AT OCEAN SCALE

Design Parameter	
Radius (R)	6 m
Hydrofoil chord (c)	6 m
WEC submergence (y_c)	12 m
Span (S)	60 m
Number of blades	2
Hydrofoil profile	NACA0015
Reynolds number for drag calculation	1e6

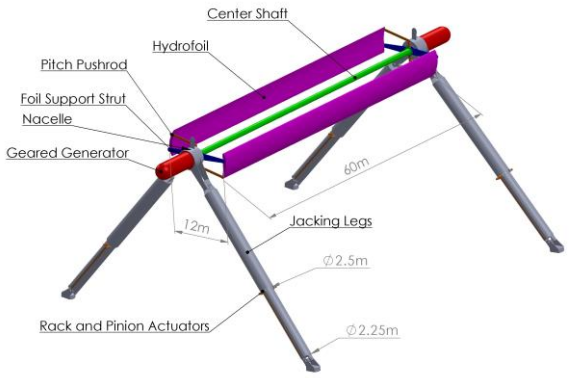

Figure 2: 3D model of the ocean scale CycWEC showing different components of the mechanical design.

B. Potential flow model

A detailed explanation of the potential flow model used in this paper can be found in Siegel et al. [9]. In its simplest form, the hydrofoil was approximated by a point vortex of strength Γ, equal to the foil circulation.

If the vortex is in the presence of a free surface it is imperative that appropriate physical boundary conditions be satisfied on the free surface. Neglecting higher order terms, the kinematic boundary condition ensuring the vertical velocity of the free surface and the fluid are equal is

$$\frac{\partial \eta}{\partial t} = \frac{\partial \phi}{\partial y} \quad (1)$$

where η is the surface elevation and ϕ is the velocity potential. The dynamic boundary condition ensuring the pressure on the free surface is atmospheric is determined from Bernoulli's equation. Substituting the free surface elevation for y, and again neglecting higher order terms results in

$$\eta = -\frac{1}{g}\frac{\partial \phi}{\partial t} \quad (2)$$

where g = 9.81 ms^{-2} is the gravity constant. Due to linearization, equation (2) can be imposed at y=0. At the up-wave and down-wave integration boundaries, the waves within the domain are allowed to leave the domain freely using a non-reflective boundary condition.

Subject to the above boundary conditions, the complex potential for a vortex moving under a free surface with position c(t) = x(t) + iy(t) in the complex plane was developed by Wehausen and Laitone [15]:

$$F(z,t) = \frac{\Gamma(t)}{2\pi i}\ln\left[\frac{z-c(t)}{z-\bar{c}(t)}\right] + \frac{g}{\pi i}\int_0^t\int_0^\infty \frac{\Gamma(\tau)}{\sqrt{gk}} e^{-ik(z-\bar{c}(\tau))} \times \sin\left[\sqrt{gk}(t-\tau)\right] dk\, d\tau \quad (3)$$

where F(z,t) is the complex potential, Γ(t) is circulation of the vortex, and k is the wave number.

It is important to note that (3) is valid for deep water waves. The circulation Γ(t) was described in a time dependent fashion, which usually requires shed vorticity in the wake. However, the effect of the wake was neglected in the current analysis as the hydrofoils eventually achieved a steady circulation in the case of harmonic analysis.

In previous work by Hermans et al. [8] a hydrofoil under a free surface was modelled by numerically integrating (3) and the results were compared to steady flow experiments with good agreement. A similar approach was employed in the current work and (3) was integrated using second order time and wave number marching techniques. Subsequently, (2) was used to determine the resulting surface elevation and wave pattern. Using superposition, this approach was further extended to a WEC with multiple hydrofoils, where the complex potential of each hydrofoil was represented by (3). The total potential is determined $\phi_{total} = \sum_{i=1}^{n} \phi_i$ where n is the total number of hydrofoils, which was 2 in the current work.

The positions of the two vortices were prescribed as a function of time. The coordinates for a vortex moving about a center of rotation (0, y_c) with radius R and frequency ω including a position offset θ relative to the incoming wave were,

$$x(t) = Rcos(\omega t + \theta) \quad (4)$$
$$y(t) = y_c - Rsin(\omega t + \theta)$$

Linear Airy wave theory was used to represent incoming and WEC generated waves. Typically, the CycWEC created more than a single plain traveling wave. The wave height of each generated wave component could be determined by Fourier analysis. It was thus possible to determine the power associated with each wave P_{Airy} by employing Airy wave theory which related wave power per unit length to wave height and period by:

$$P_{Airy} = \frac{1}{8}\rho g H^2 C_g = \frac{1}{32}\rho g^2 H^2 T \quad (5)$$

where ϱ = 1000 kgm^{-3} was the density of water, g = 9.81 ms^{-2} the gravity constant, C_g the wave group velocity and H the Airy wave height. Since the wave power scaled linearly with the wave period T, higher harmonic waves of the same wave height contained less energy in proportion to their period. Also, there was a quadratic relationship between wave energy and wave height H.

The only CycWEC generated wave that interacted with an incoming Airy wave and extracted power was the fundamental wave of the same frequency. The rest of the harmonics generated by the CycWEC contributed to the power losses. Besides this, any waves that travelled in the up-wave direction also did not contribute to power extraction. The wave power analysis was based on energy conservation, which was implicit in the unsteady Bernoulli equation, and a control volume analysis assuming that all energy leaving or entering at the up-wave and down-wave boundaries was contained in traveling Airy type waves. Thus, the power difference at both boundaries must be absorbed by the traveling point vortices, equal to the inviscid power generated by the CycWEC.

Based on this, one figure of merit for WEC design was the ratio of the power in the fundamental wave traveling in the positive X direction, P_1, compared to the power contained in all other waves,

$$\frac{P_1}{P_{all}} = \frac{P_1}{\sum_{n=-\infty}^{\infty} P_n} \quad (6)$$

The losses because of harmonic and up-wave traveling waves were referred to as harmonic losses, defined as $P_{harm} = 1 - P_1/P_{all}$. The inviscid shaft power was calculated as:

$$P_{Sinv} = (P_{Airy} - P_{1rem}) - P_{harm} \quad (7)$$

where P_{1rem} was the fundamental wave power remaining at the down-wave location and was given by subtracting P_1 from P_{Airy}. Thus, the cancelled power was $P_{cancel} = P_{Airy} - P_{1rem}$. The inviscid efficiency of wave cancellation was given by the ratio of inviscid shaft power to the incoming wave power

$$\eta_{inv} = \frac{P_{Sinv}}{P_w} \quad (8)$$

The amount of circulation required to generate a particular fundamental wave height was also of importance, defined as H_1/Γ. Since the fundamental wave height was linearly related to circulation as shown in Siegel et al. [9], the amount of circulation required to cancel

a wave of a given wave height could be calculated once H_1/Γ had been determined for a wave period of interest.

C. Viscous loss estimate

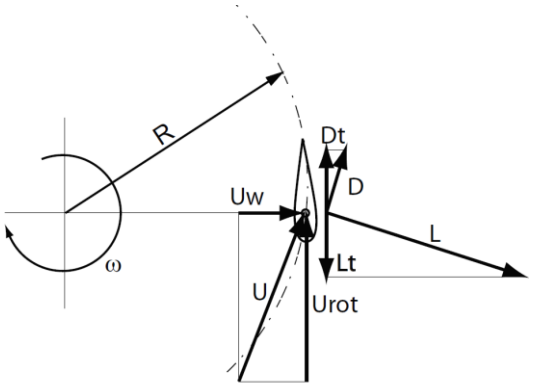

Fig. 3: Forces acting on a rotating hydrofoil of the CycWEC [8].

Since the above described numerical model gave inviscid 2-D results, viscous loss needed to be estimated to determine shaft power. For any two-dimensional hydrofoil, the relationship between circulation and lift was:

$$\Gamma = 0.5\, C_L\, U_f\, c \tag{9}$$

$$C_L = \frac{L}{\frac{1}{2}\rho {U_f}^2 c} \tag{10}$$

where c was the hydrofoil chord, C_L the non-dimensional lift coefficient, U_f the velocity of the foil, and L the lift force created by the foil per unit span. Based on the lift coefficient C_L, the drag coefficient C_D could be easily calculated for a particular hydrofoil shape with panel codes that were available in the open source. This relationship between C_L and C_D is called the drag polar of the hydrofoil. To calculate this relationship, we used XFOIL panel code [16]. This was done outside of our numerical scheme, and the generated results were used in our analysis to calculate the drag losses. This drag coefficient C_D accounted for the parasitic drag which consisted of the form drag and the skin friction drag due to viscosity. If because of the chosen CycWEC geometry and rotational period, the required circulation could not be achieved before reaching the stall angle of attack, the circulation was limited to the value achieved just before hydrofoil stall. In this situation, perfect wave termination would not be achieved, but rather a reduced residual fundamental wave height H_1 would be found down–wave of the CycWEC.

Along with the viscous drag, the hydrofoils also experienced a lift induced drag due to their finite span [17]. This drag could be calculated by:

$$C_{di} = \frac{{C_L}^2}{\pi e AR} \tag{11}$$

where C_{di} was the induced drag coefficient, e the span efficiency factor which was assumed to be 0.9, and AR the aspect ratio of the foil. The value of AR was 10 for the present investigation.

The obtained lift and drag coefficients were used to calculate the shaft torque and thus power loss due to the tangential component of the drag force, $P_d = D_t R\omega$, Fig. 1 shows that this power reduced the shaft power available. Using a conservation of energy approach, the power available at the shaft P_{SD} of the CycWEC could be calculated as:

$$P_{SD} = (P_{Airy} - P_1) - P_{harm} - P_{d0} - P_{di} \tag{12}$$

The power delivered to the shaft P_{SD} was defined as the portion of the wave power cancelled by the WEC, minus the losses from other (harmonic) waves generated, minus the losses from the parasitic drag and the induced drag. Note that all powers and power losses were multiplied by the span of the CycWEC to get total power generation. The efficiency of power generation was the ratio of generated shaft power to incoming wave power given by:

$$\eta_{SD} = \frac{P_{SD}}{P_w} \tag{13}$$

This shaft power did not consider other effects like bearing friction, generator and other electrical losses. Previously it was shown in [18] that the 3-dimensional radiation patterns of the waves generated by the CycWEC have an effect on the shaft power. In the following analysis, the 3-dimensional wave radiation effects were not considered. A detailed discussion on these 3-D wave radiation effects of the CycWEC can be found in [19].

D. Irregular waves

One way to represent irregular waves was by using a spectral or Fourier model. Under this approximation, irregular waves could be viewed as the superposition of a number of regular waves (wave components) with different frequencies and amplitudes. A parameter called significant wave height, H_s, was defined as the average of the highest 1/3 of the waves. Similarly, the peak period, T_p, was defined as the period of the highest energy wave. These parameters are commonly used for a representative wave to approximate the otherwise random field. In this paper, we used the JONSWAP spectrum to approximate incoming irregular waves [20]. In the current analysis, the significant wave period (T_s) was approximately equal to the peak period of the spectrum.

The power P_{irr} in a typical irregular ocean sea state as recorded in the buoy data could be approximated by:

$$P_{irr} = \frac{1}{64\pi}\rho g^2 H_s^2 T_p \tag{14}$$

The shaft power needed to be calculated in a different manner than for regular waves. Since for irregular waves, each incoming wave had a different height and period, the harmonic losses could not be calculated directly. Instead, Fourier analysis of the entire time histories of surface elevation up-wave and down-wave were used to get the

total power contained in waves entering and leaving the control volume. Similarly, as before, the difference between these two values was the inviscid shaft power.

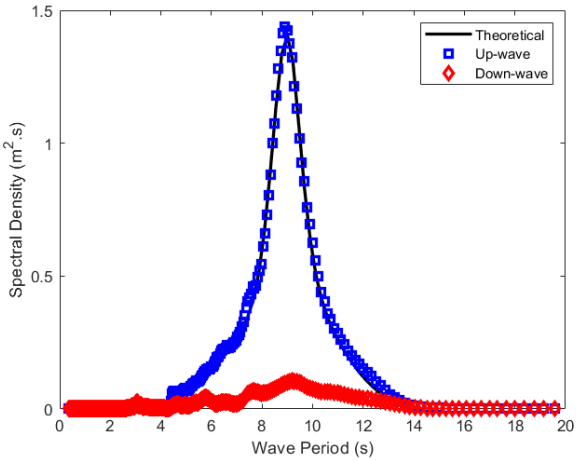

Fig. 4: Comparison of wave spectra at up-wave and down-wave locations with a theoretical JONSWAP wave spectrum at a significant wave period of 9s.

Fig. 4 shows wave spectra for an irregular wave cancellation simulation at a significant wave period of 9s. The up-wave spectrum of the incoming wave matched closely with the theoretical JONSWAP spectrum. The spectral density magnitude from the down-wave spectrum was significantly smaller than that of the up-wave spectrum. This indicates that the CycWEC was able to cancel incoming irregular waves effectively at a high inviscid efficiency.

Because of the time varying nature of circulation and foil velocity, the drag losses were not constant for irregular wave simulations. To estimate overall drag loss, a simple time average of the drag power losses was used.

E. Feedback control

Since for irregular waves, each incoming wave had a different height and period, the CycWEC needed to adjust its blade pitch and rotational speed to extract maximum amounts of energy from the incoming wave. This was done through a feedback control algorithm which used estimation of the incoming wave to control the blade pitch, rotational position and speed of the blades.

It was also important to control the blade pitch from a standpoint of drag losses. One control strategy could be trying to cancel the maximum amount of incoming wave height by pitching the blades to create high enough circulation. This approach was called controller 1 and was used in earlier published work. In this case, the inviscid power extracted by the CycWEC was maximized, but the power generated after considering viscous losses would be small. The reason for this was twofold. The first reason was that the parasitic drag to lift relationship from the drag polar is not linear. As the blades were pitched more and more, the circulation and the lift of the hydrofoil increased. This increase in lift caused an even greater increase in the parasitic drag, increasing the loss associated with it. Similarly, from (11) it could be seen that the induced drag scales as a quadratic function of the lift. This meant that as lift increased, the induced drag also increased at a larger rate, increasing the power loss associated with it. Thus, when both drag losses were considered, maximizing inviscid efficiency could cause huge drag power losses, leading to minimal to no shaft power in some cases.

In the other control approach, the viscous losses could be estimated *a priori* from the circulation needed to generate a particular wave height. A simple optimization could be done to find values of blade pitch and circulation to maximize the total shaft power (P_{SD}). This approach was called controller 2. With this approach, the inviscid efficiency of the WEC could be lower, but the power generated after considering viscous losses would be larger than controller 1. In the first approach, the controller tried to optimize inviscid wave cancellation, and in the second approach the controller tried to maximize shaft power.

Table 2 shows the results obtained with these two control approaches for a regular wave with a height of 2m and a period of 10s. Controller 1 gave better inviscid results but barely produced any shaft power after drag losses were considered.

TABLE 2
EFFICIENCY AND SHAFT POWER WITH THE TWO CONTROL APPROACHES FOR REGULAR WAVE CANCELLATION SIMULATION WITH AN INCOMING WAVE HEIGHT OF 2M AND A WAVE PERIOD OF 10S.

	η_{inv}	P_{sinv} (kW)	η_{SD}	P_{SD} (kW)
Controller 1	81.4%	1869.6	0.9%	21.4
Controller 2	55.9%	1283.4	28.1%	645.0

Controller 2 gave worse inviscid results, but produced considerably larger shaft power after drag losses were considered, nearly 30 times more than controller 1 for this case.

F. Climate scatter

Wave climate data from Humboldt Bay, CA was used to calculate the performance of the CycWEC under different sea states. The buoy data for this location is available on the internet [21]. The scatter diagram in Fig. 5 shows the actual hours per year for which a sea state was present in that year and the annual wave energy resource which was obtained by multiplying the hours per year of a sea state by its wave energy calculated from (5) and shown in Fig. 6.

For the power matrix runs performed, total energy generated per year by the CycWEC could be calculated by appropriately summing energy generated for each sea state. An overall yearly efficiency could be calculated by comparing this energy generated per year to available energy per year. From the scatter diagram shown in Fig. 5, the total annual energy available was 210 MWh or an average wave power of 30kW, both values per meter of wave crest.

Since the climate data were in terms of significant wave height and significant wave period, they could readily be used for irregular simulations. However, it was also possible to estimate the annual energy generation from

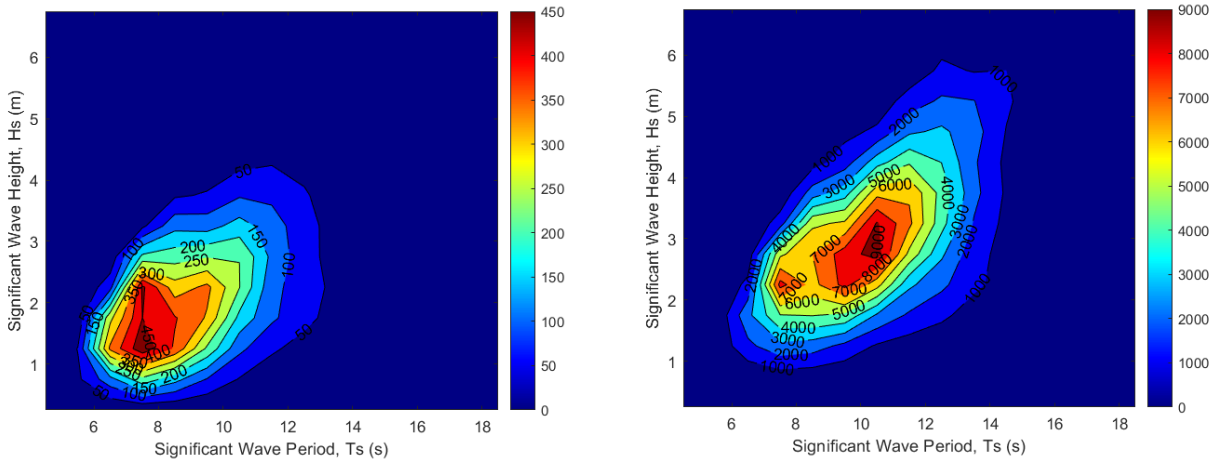

Fig. 5: Total hours per year of different sea states from (left), and total available energy resource for each sea state in kWh per meter of wave crest per year (right). Data from Humboldt Bay, CA [18].

regular wave simulations. By comparing equations (14) for irregular wave power and (5) for Airy wave power, it could be argued that for matching wave powers, $H_s = \sqrt{2}H_{Airy}$. Using this relation, the wave climate could be applied to regular wave simulations to calculate annual energy generation and efficiency.

It is interesting to note that even though the most frequent sea state was T_s = 7.5s and H_s = 1.25m, more energy per year was available at a sea state of T_s = 10.5s and H_s = 2.75m. Thus, it would be wrong to adopt the most frequent sea state as the design point if the objective is to generate the maximum amount of energy per year with a wave energy converter.

III. Simulation Results

Based on the numerical scheme described above, simulations were run at different sea state conditions for various combinations of wave heights and wave periods. The total incoming wave power per unit meter of the wave crest available for cancellation is shown in Fig. 6 for both regular and irregular waves. Because of $H_s = \sqrt{2}H_{Airy}$ relationship, a maximum wave height for regular waves of 4.75m was used, whereas the maximum significant wave height for irregular waves was 6.25m.

To get sufficient temporal resolution, a time step 50 times smaller than the wave period was used ($\Delta t = \frac{T}{50}$). Since equation (3) needs to be solved numerically, integrating the wave number to infinity was impossible. Convergence studies were run to determine maximum wavenumber (k_{max}) and the wavenumber step (Δk). k_{max} value equal to 100 times the wave number of the incoming wave ($k_{max} = 100 * k_{wave}$) and Δk value 20 times smaller than wave number of the incoming wave ($k_{wave}/20$) gave sufficiently converged results within 1% of further refinement.

A. *Regular waves*

For regular wave cancellation runs, wave heights ranged from 0.25m to 4.75m with an increment of 0.25m, and wave periods ranged from 5s to 16s with an increment of 1s. In total, 120 different combinations of wave heights and wave periods were simulated. The details of the geometry of the WEC were as given in Table 1.

Since the efficiency of the CycWEC depends on cancelled wave power and other power losses as given in

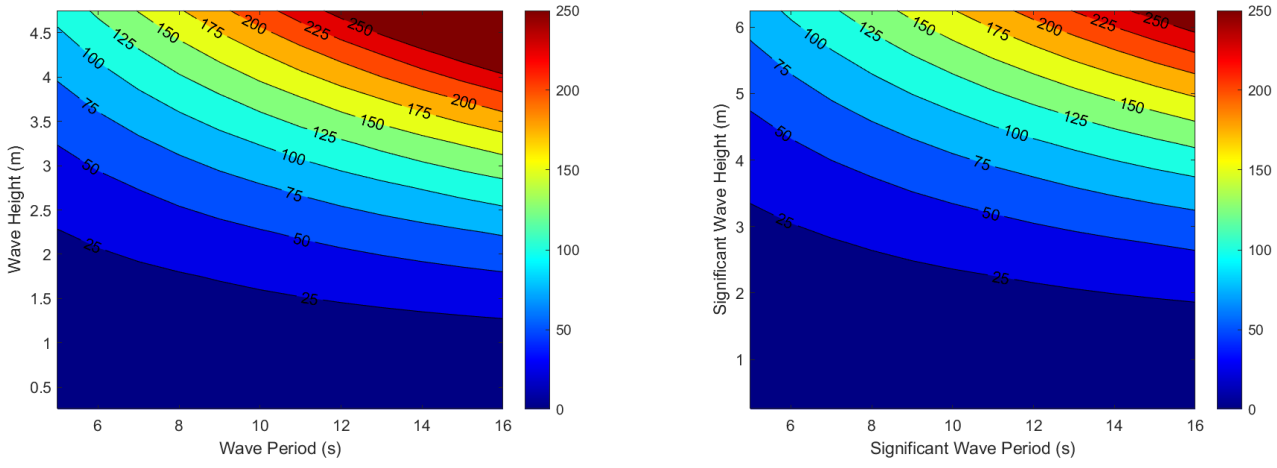

Fig. 6: Available wave power per unit span at different sea states. Left, regular wave conditions. Right, irregular wave conditions. Units are kW per meter of wave crest.

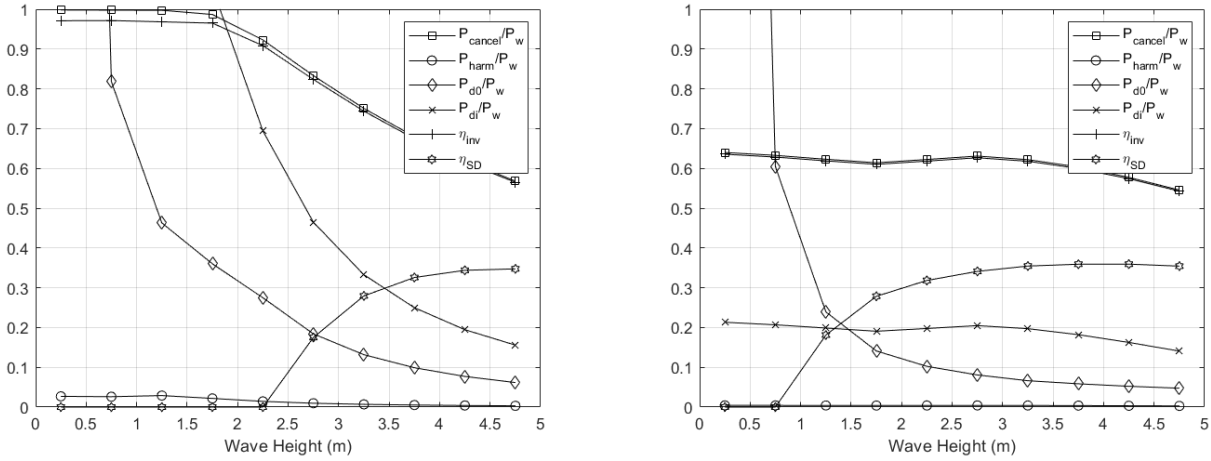

Fig. 7: Cancelled wave power, harmonic and drag power losses normalized with incoming wave power and inviscid and total efficiency of power conversion for the CycWEC at a wave period of 9s. Left, controller 1, Right, controller 2.

(12), it was important to understand their relationship in detail for specific wave periods and wave heights. It is also important to understand how these quantities change with the two control approaches. Fig. 7 plots different powers relative to incoming wave power and efficiencies for a fixed wave period of T = 9s for controller 1 (left), and controller 2 (right) With controller 1, the ratio of cancelled wave power to incoming wave power and inviscid efficiency remained higher than 0.9 till a wave height of 2m. As the wave height increased further, the circulation and lift required to completely cancel the incoming wave became larger than the values at stall. Since these values could not be exceeded, any further increase in incoming wave height showed a decrease in inviscid performance of the CycWEC. The harmonic losses remained negligible for all wave heights. As clear from the plot, the main power losses were because of parasitic and induced drag. At relatively small wave heights, the drag losses exceed the cancelled wave power resulting in negative shaft power. This means that the rotation of the CycWEC could not be sustained at these wave heights without supplying external power. As wave height was increased, both drag losses decreased relative to the incoming wave power. The primary reason for this was that the incoming wave power increased with the square of the wave height as seen in (5). Beyond a certain wave height, the drag losses remained constant as the maximum circulation before reaching stall was achieved and no further increase in lift or drag could be obtained. This effectively reduced the ratio of drag power losses to the incoming wave power for larger wave heights. The combined effect of these losses exceeded the cancelled shaft power until the incoming wave height increased beyond a certain threshold. This threshold can be thought of as a cut-in wave height for the CycWEC beyond which positive shaft power could be generated. With controller 1, this cut-in wave height was quite large at 2.25m. The maximum shaft efficiency (η_{SD}) achieved was 35% at a wave height of 4.25m. With controller 2, the inviscid efficiency remained steady near 60% for most of the wave heights. The harmonic losses were negligible, as with controller 1. The major differences were with the induced drag loss which never exceeded a quarter of the incoming wave power with controller 2. The parasitic drag loss also showed a steeper drop in its value compared to controller 1. Because of these losses being smaller, the cut-in wave height with controller was 0.75m which was a drastic reduction compared to controller 1. This underlines the fact that controller 2 could produce power at a larger

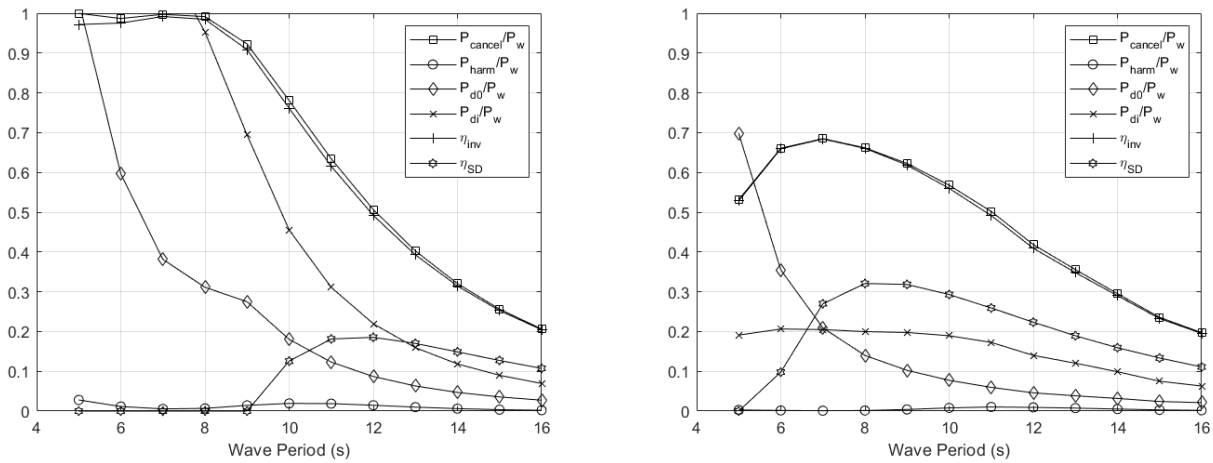

Fig. 8: Cancelled wave power, harmonic and drag power losses normalized with incoming wave power and inviscid and total efficiency of power conversion for the CycWEC at a wave height of 2.25m. Left, controller 1. Right, controller 2.

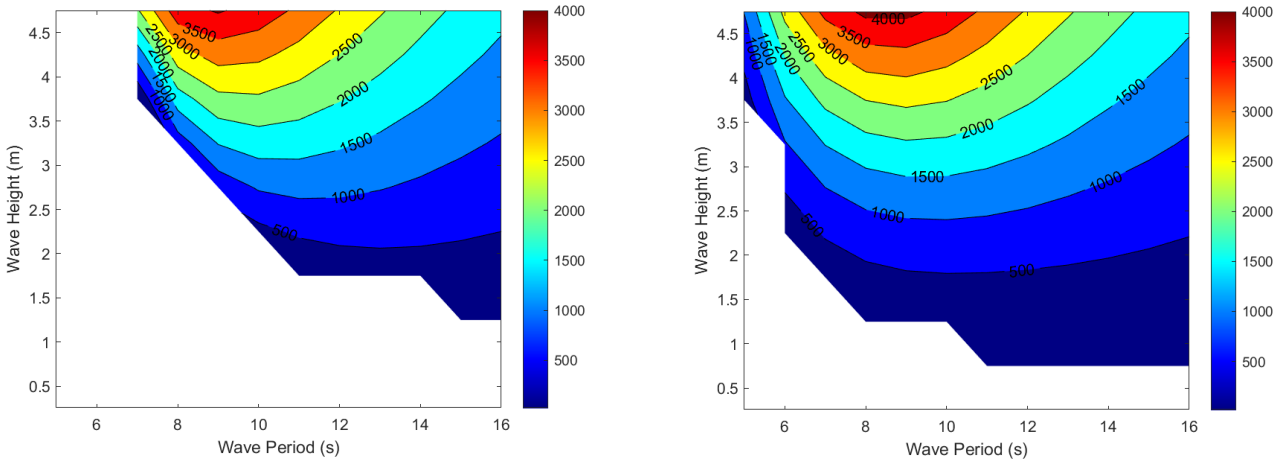

Fig. 9: Estimated shaft power generated after losses were considered for regular wave simulations. Left, controller 1. Right, controller 2. Units in kW.

number of wave conditions because of its ability to minimize the drag losses. The maximum shaft efficiency was 36% at a wave height of 3.25m, which was similar to controller 1.

Fig. 8 plots the same quantities as in Fig. 7 for a fixed wave height of H = 2.25m for both control approaches. With controller 1, the ratio of cancelled wave power to incoming wave power, and the inviscid efficiency were greater than 0.95 for wave periods less than 8s and then decreased thereafter. This can be explained as follows. As the wavelength of the incoming wave increased, the CycWEC diameter to wavelength ratio moved further away from the optimal value of $2R/\lambda = 1/\pi$ as established in [9]. At larger wavelengths, the rotational velocity of the hydrofoils decreased, reducing their circulation. Both these effects contributed to a decrease in the inviscid performance at larger wave periods. The harmonic losses remained negligible for all wave periods. The relative drag losses again showed a decreasing trend with increasing wave periods. The drag losses were smaller at larger wave periods, since they were directly proportional to the rotational speed of the hydrofoils. The incoming wave power increased proportional to the increasing wave period as seen in (5). Both these effects reduced drag losses relative to the incoming wave power at larger wave periods. With controller 1, for wave periods smaller than 10s, the CycWEC could not produce positive shaft power because of larger drag losses than cancelled wave power. The maximum shaft efficiency (η_{SD}) was close to 20% at a wave period of 12s. With controller 2, the maximum inviscid efficiency was 70%, however, the induced drag power loss to incoming wave power ratio never exceeded 0.2. Because of the lower drag losses, the CycWEC was able to produce positive shaft power at all wave periods larger than 5s with controller 2. The maximum shaft efficiency was 31% at a wave period of 8s. This again highlights the fact that controller 2 gave overall better performance than controller 1 when drag losses were considered.

Fig. 9 shows the scatter plots of total power generated (P_{SD}) per unit span of the CycWEC with controller 1 (left) and controller 2 (right). The white parts of the plots show the sea state at which the CycWEC was unable to produce positive shaft power. The cut-in wave height of the CycWEC decreased as the wave period increased. This was because the drag losses relative to the wave power decreased with increasing wave period and the CycWEC was able to produce positive shaft power at smaller incoming wave heights. The large drag losses at smaller

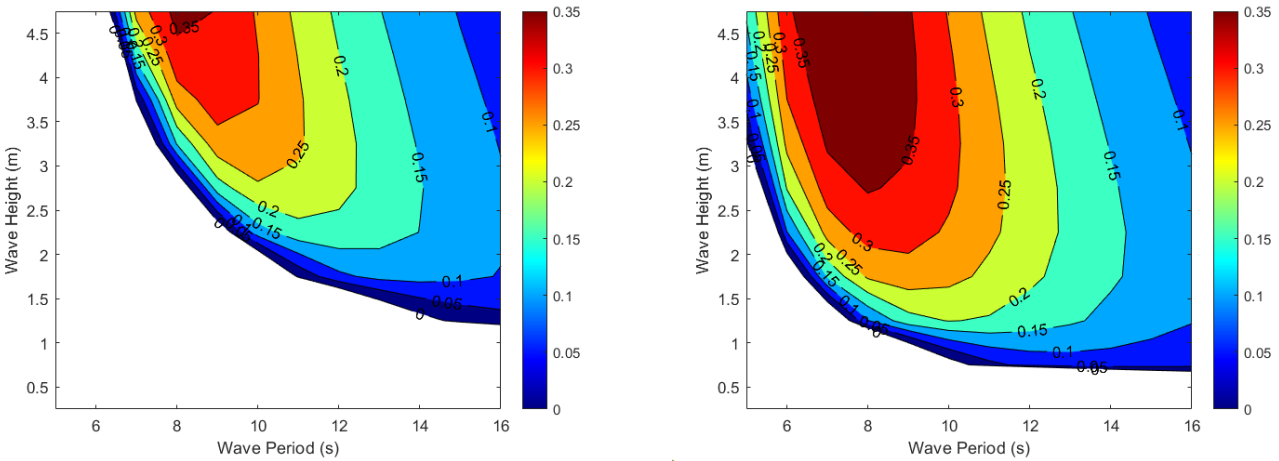

Fig. 10: Efficiency of power generation after harmonic and drag losses were considered for regular wave simulations. Left, controller 1. Right, controller 2.

wave periods caused a larger cut-in wave height. Even though this behaviour was similar for both control approaches, the cut-in wave heights with controller 2 were smaller than with control controller 1 for the same wave period. This meant that controller 2 could produce positive shaft power at a larger number of sea states than controller 1. The maximum shaft power generated was approximately 4.1MW for both approaches at a wave period of 9s and a wave height of 4.75m. This sea state was different than where maximum power was available, which was at a wave period of 16s and a wave height of 4.75m, from Fig. 6. This was mainly due to the inability of the CycWEC to generate enough circulation at larger wave periods being limited by hydrofoil stall.

Fig. 10 shows the scatter plots of total shaft efficiency of power conversion (η_{SD}) obtained with controller 1 (left) and controller 2 (right). At most of the sea states, controller 2 produced more shaft power at a higher shaft efficiency than controller 1. The maximum shaft efficiency was 36% with controller 1 and 40% with controller 2, at a wave period of 8s and a wave height of 4.75m. The total energy generated per year was calculated by using the number of hours each sea state was active in a year from Fig. 5 and summing up energy generated at all sea states. Table 3 shows the total energy generated per year and yearly efficiency of energy generation for both control approaches. With controller 2, the annual shaft energy generated and the bulk yearly efficiency was more than double than with controller 1.

TABLE 3
ESTIMATED ANNUAL ENERGY GENERATION AND YEARLY EFFICIENCY FOR THE CYCWEC WITH REGULAR WAVES

Control Strategy	Total Energy Generated (MWh/year)	Yearly Efficiency
Controller 1	1299.6	9.4%
Controller 2	2953.9	21.5%

B. Irregular waves

For irregular wave cancellation simulations, significant wave heights ranged from 0.25m to 6.25m, and significant wave periods ranged from 5s to 16s. In total, 156 combinations of significant wave height and period were simulated. The JONSWAP spectrum used 40 different wave components in the wave period range of $0.5*T_s$ to $1.5*T_s$.

Since a JONSWAP spectrum was used to approximate irregular waves, the simulations needed to run for a long enough time for the spectrum to converge to the estimated wave power. For this analysis, simulations were solved for time equal to 100 times the specific wave period of the spectrum. Solving the simulations for longer time spans gave results within 2% of the results presented here, indicating that the simulations had converged sufficiently for the purpose of this investigation.

To demonstrate the difference between regular and irregular wave cancellation results, Fig. 11 shows the surface elevations of the incoming wave, the CycWEC generated waves and the total resultant surface elevation at a sensing location two wavelengths down-wave from the CycWEC. For regular waves, the surface elevations reached a steady periodic pattern after a few cycles. The irregular waves showed fluctuating behaviour with no discernible pattern. This was expected since we used a JONSWAP spectrum to represent irregular waves with a randomized phase for each wave component. With proper control of blade pitch and phase, the CycWEC produced waves that were out of phase with the incoming wave, resulting in wave cancellation. This is clear from the total resulting surface elevation, which was typically much smaller than the incoming wave surface elevation.

Similar to regular wave simulations, the performance of the CycWEC was evaluated for each significant wave period and a significant wave height. Fig. 12 plots the different power ratios and efficiencies at a fixed significant wave period of 9s. Since the resulting incoming waves did not have a constant wave period, the harmonic losses could not be separated into individual harmonic waves. However, their effect was included in the inviscid shaft power (P_{sinv}). With controller 1, the inviscid efficiency remained high, close to 90% for significant wave heights

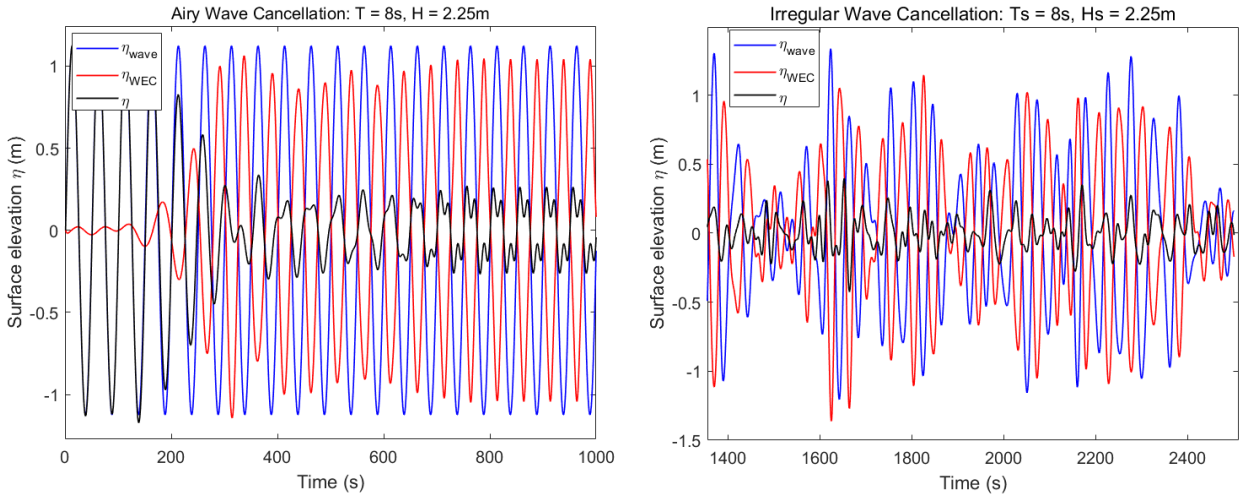

Fig. 11: Downstream surface elevations of an incoming wave, surface elevation generated by the CycWEC and total resulting surface elevation for regular wave cancellation (left) and irregular wave cancellation (right), as an example.

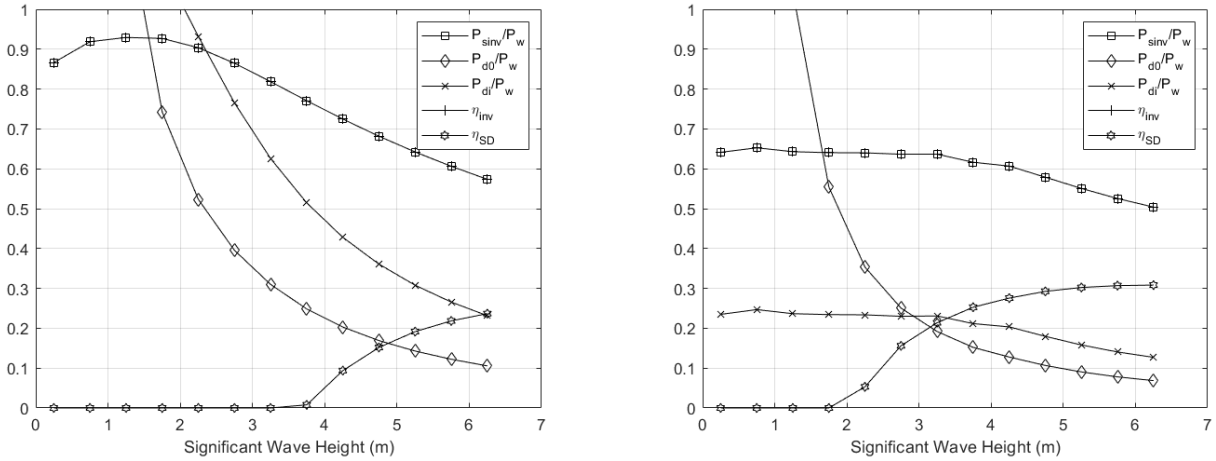

Fig. 12: Cancelled wave power, drag power losses normalized with incoming wave power and inviscid and total efficiency of power conversion for the CycWEC from irregular wave simulations at a constant significant wave period, Ts = 9s. Left, controller 1. Right, controller 2.

less than 2.25m, after which it started declining. The reasons for this were identical to the ones described for regular wave simulations. The drag losses also showed similar decreasing behaviour with increasing H_s. The CycWEC produced positive shaft power for significant wave heights larger than 3.5m, which can be considered as the cut-in significant wave height for this T_s. With controller 2, the inviscid efficiency remained flat close to 60% for all H_s smaller than 4.75m, decreasing slightly afterwards. The drag losses showed significant reductions compared to controller 1. The ratio of induced drag power to incoming wave power never exceeded 0.25, which was significantly less than with controller 1, especially at smaller H_s values. The cut-in significant wave height with controller 2 was 1.75m, which was considerably smaller than with controller 1, showing the improvement in performance. The maximum shaft efficiency (η_{SD}) was 30% with controller 2 which was better than 25% with controller 1. Both these maximum values were obtained at a H_s of 6.25m.

Fig. 13 plots the power ratios and efficiencies for a constant significant wave height of 2.25m. With controller 1, the inviscid efficiency peaked at 95% at a T_s of 7s, decreasing thereafter. The drag losses remained high for most of the values of T_s and the CycWEC did not produce positive shaft power for significant wave periods less than 15s with controller 1. Controller 2 showed smaller inviscid efficiency with a maximum of 68% at a T_s of 8s. However, the drag losses were again much smaller compared to controller 1. The CycWEC was able to produce positive shaft power for all significant wave periods larger than 8s with controller 2. The maximum shaft efficiency was 5% with controller 1 at a T_s of 16s and 17% with controller 2 at a T_s of 12s.

Fig. 14 shows scatter plots of total shaft power (P_{SD}) for irregular wave simulations with controller 1 and controller 2. The area of the plot where the CycWEC was unable produce positive shaft power increased compared to the regular wave simulations. Controller 2 again produced shaft power at a greater number of conditions than controller 1, showing the importance of minimizing drag losses. The maximum shaft power produced was 2.48 MW with controller 1 and 2.8 MW for controller 2, both obtained at a H_s of 6.25m and a T_s of 10s.

Fig. 15 plots the shaft efficiency for irregular wave simulations. The maximum efficiency was 32% with

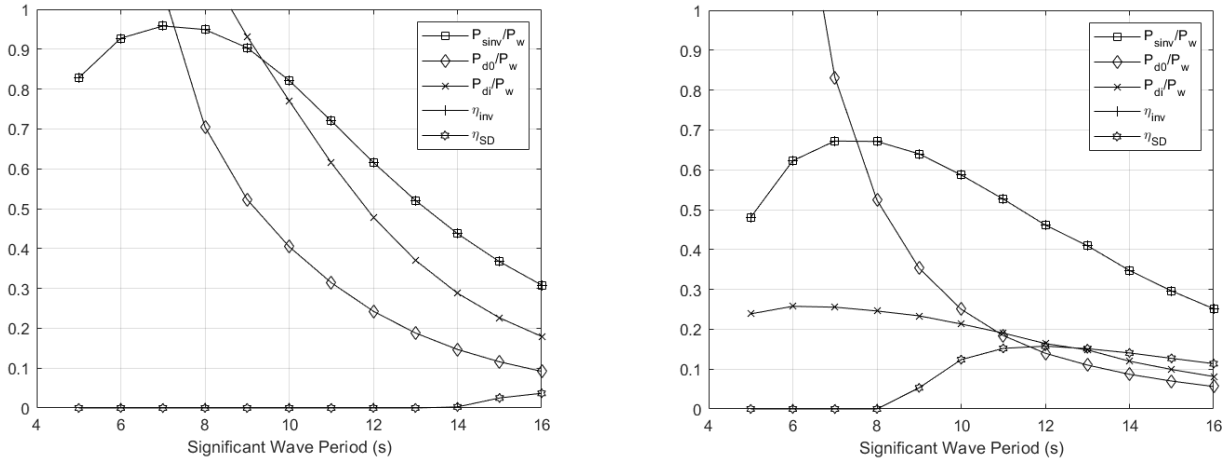

Fig. 13: Cancelled wave power, drag power losses normalized with incoming wave power and inviscid and total efficiency of power conversion for the CycWEC from irregular wave simulations at a significant wave height, Hs = 9s. Left, controller 1. Right, controller 2.

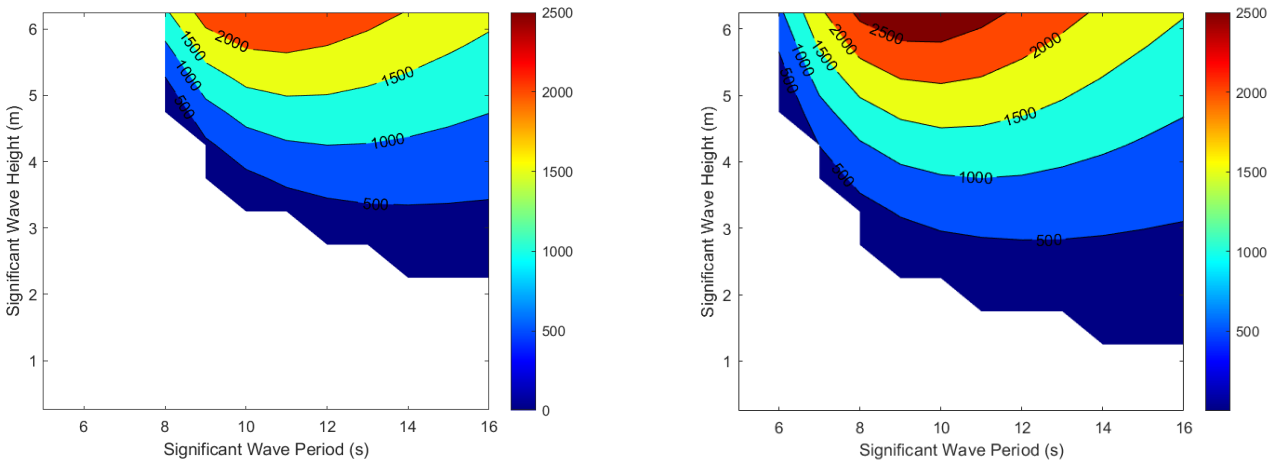

Fig. 14: Estimated shaft power generated per unit span after losses were considered for irregular wave simulations. Left, controller 1. Right, controller 2. Units in kW.

controller 2, whereas it was only 24% with controller 1. Compared to controller 1, controller 2 was able to produce more shaft power at a higher shaft efficiency for most of the sea states. This behaviour was consistent with the results from regular wave simulations. Table 4 shows estimated annual total energy generated and yearly efficiency for irregular waves. Controller 2 nearly tripled the energy generation and efficiency compared to controller 1. Compared to regular wave simulations, the efficiency of energy generation was lower with both control approaches. The primary reason for this is believed to be some spurious behaviour in the estimation algorithm causing an unintended increase in drag losses as the CycWEC tries to adjust the blade pitch based on these data. Currently efforts are ongoing to eliminate this behaviour and improve the performance of the CycWEC for irregular waves.

TABLE 4
ESTIMATED ANNUAL ENERGY GENERATION AND YEARLY EFFICIENCY OF THE CYCWEC WITH IRREGULAR WAVES

Control Strategy	Total Energy Generated (MWh/year)	Yearly Efficiency
Controller 1	714.8	5.66%
Controller 2	1800.8	14.26%

IV. CONCLUSIONS

Performance of an ocean scale design of a CycWEC with a radius and a chord of 6m, and a span of 60m was evaluated for regular and irregular waves using numerical simulations. Annual energy generation and bulk yearly efficiency were estimated based on wave climate data from Humboldt Bay, CA. Two different control approaches were used for wave cancellation. The first control approach (controller 1) maximized the inviscid efficiency by trying to cancel as much as possible of the incoming wave height, thus maximizing inviscid wave energy extraction. The second control approach (controller 2) controlled the blade pitch to minimize the viscous and induced drag losses. The results show a dramatic two-fold increase in shaft power with controller 2, underlining the importance of considering drag losses in the control approach. The irregular wave simulations showed similar but slightly reduced efficiencies compared to the efficiencies of the regular wave simulations. This leaves room for further improvement by optimizing the control algorithm for irregular wave cancellation.

The estimated yearly efficiency was 21% from regular and 14% from irregular wave simulations. The estimated

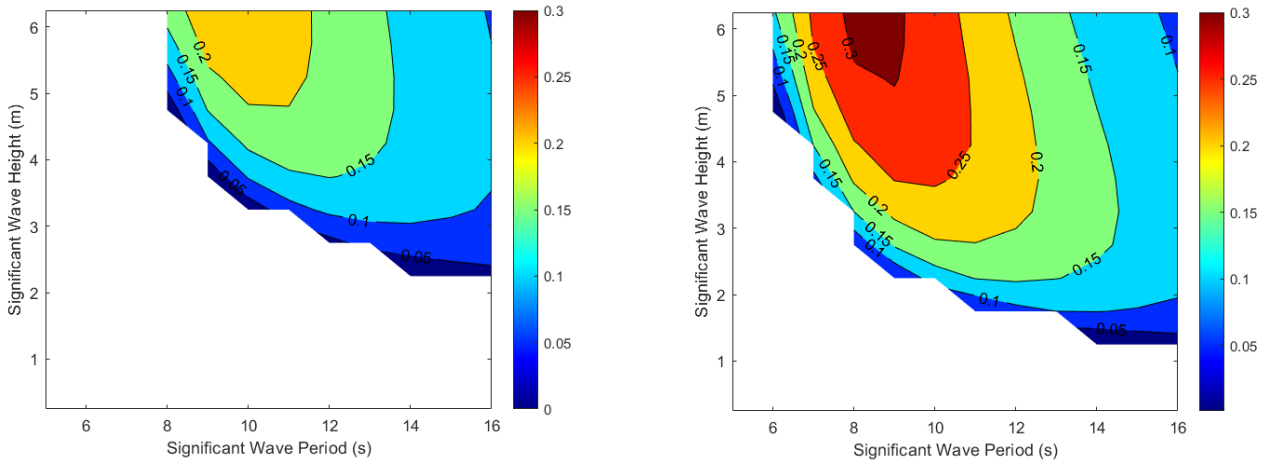

Fig. 15: Efficiency of power generation after drag losses were considered for irregular wave simulations. Left, controller 1. Right, controller 2.

annual energy generation of the CycWEC was 3000 MWh for regular, and 1800MWh for irregular waves. The estimated maximum shaft power production was close to 4.8MW for regular, 2.5MW for irregular waves. Future developments in estimation and control algorithms will further enhance the CycWEC's performance for irregular waves. This makes the CycWEC a commercially viable option to extract energy from ocean waves.

Disclaimer

This report was in part prepared as an account of work sponsored by an agency of the United States Government. Neither the United States Government nor any agency thereof, nor any of their employees, makes any warranty, express or implied, or assumes any legal liability or responsibility for the accuracy, completeness, or usefulness of any information, apparatus, product, or process disclosed, or represents that its use would not infringe privately owned rights. Reference herein to any specific commercial product, process, or service by trade name, trademark, manufacturer, or otherwise does not necessarily constitute or imply its endorsement, recommendation, or favoring by the United States Government or any agency thereof. The views and opinions of the author expressed herein do not necessarily state or reflect those of the United States Government or any agency thereof.

Acknowledgments

The authors would like to thank Ms. Freia Siegel for proofreading the paper. This material is partially based upon work supported by the Department of Energy under Award Number DE-EE0008626.

References

[1] G. Boyle, Renewable Energy - Power for a sustainable future, Oxford University Press, 2004.

[2] "Mutriku Wave Power Plant," [Online]. Available: https://tethys.pnnl.gov/project-sites/mutriku-wave-power-plant. [Accessed 2021].

[3] M. McCormick, Ocean Wave Energy Conversion, John Wiley & Sons, 1981.

[4] J. Cruz, Ocean wave energy: current status and future perspectives, Springer-Verlag, 2008.

[5] E. Rusu and F. Onea, "A review of the technologies for wave energy extraction," Clean Energy, vol. 2, no. 1, pp. 10-19, 2018.

[6] T. Y.-T. Wu, "Swimming of a waving plate," Journal of Fluid Mechanics, vol. 10, pp. 321-344, 1961.

[7] C. Marburg, "Investigation on a Rotating Foil for Wave Energy Conversion," 1994.

[8] A. J. Hermans, E. Sabben and J. A. Pinkster, "A device to extract energy from water waves," Applied Ocean Research Computational Mechanics Publications, Vols. Vol. 12, No. 4, p. 5, 1990.

[9] S. G. Siegel, T. Jeans and T. McLaughlin, "Deep Ocean Wave Energy Conversion using a Cycloidal Turbine," Applied Ocean Research, vol. Volume 33 Issue 2, pp. 110-119, 2011.

[10] S. Siegel, T. Jeans and T. McLaughlin, "Deep Ocean Wave Cancellation Using a Cycloidal Turbine," in 62nd Annual Meeting of the American Physical Society, Division of Fluid Dynamics, Minneapolis, MN, 2009.

[11] C. Fagley, S. Siegel and J. Seidel, "Wave Cancellation Experiments using a 1:10 Scale Cycloidal Wave Energy Converter," in 1st Asian Wave and Tidal Energy Conference (AWTEC) Jeju Island, Korea, November 27-30, 2012.

[12] T. Jeans, C. Fagley, S. G. Siegel and J. Seidel, "Irregular Deep Ocean Wave Energy Conversion Using a Cycloidal Wave Energy Converter," International Journal of Marine Energy, vol. 1, pp. 16-32, 2013.

[13] S. G. Siegel, C. Fagley and S. Nowlin, "Experimental wave termination in a 2D wave tunnel using a cycloidal wave energy converter," Applied Ocean Research, vol. 38, pp. 92-99, 10 2012.

[14] S. G. Siegel, "Wave Climate Scatter Performance of a Cycloidal Wave Energy Converter," Applied Ocean Research, vol. 48, pp. 331-343, 2014.

[15] J. V. Wehausen and E. V. Laitone, Surface Waves, Handbook of Physics, Vol.9, Springer-Verlag, 1960.

[16] M. Drela, "XFOIL: An Analysis and Design System for Low Reynolds Number Airfoils," Low Reynolds Number Aerodynamics. Lecture Notes in Engineering, vol. 54, pp. 1-12, 1989.

[17] H. Glauert, The elements of airfoil and airscrew theory, Cambridge University Press, 1947.

[18] S. G. Siegel, "Wave Radiation of a Cycloidal Wave Energy Converter," Applied Ocean Research, vol. 49, pp. 9-19, 2015.

[19] A. Mohtat, C. Fagley, K. Chitale and S. Siegel, "Efficiency analysis of the cycloidal wave energy convertor under real-time dynamic control using a 3D radiation model," in 14th European Wave and Tidal Energy Conference, Plymouth, UK, 2021.

[20] K. Hasselmann and e. al., "Measurements of wind-wave growth and swell decay during the Joint North Sea Wave Project (JONSWAP)Measurements of wind-wave growth and swell decay during the Joint North Sea Wave Project (JONSWAP)," Ergnzungsheft zur Deutschen Hydrographischen Zeitschrift Reihe, vol. A(8), no. Nr. 12, p. 95, 1973.

[21] "Station 46244, Humboldt bay," [Online]. Available: https://www.ndbc.noaa.gov/station_page.php?station=46244. [Accessed 2020].